fluids

Article

Heat Transfer Study of the Ferrofluid Flow in a Vertical Annular Cylindrical Duct under the Influence of a Transverse Magnetic Field

Panteleimon A. Bakalis [1,*], Polycarpos K. Papadopoulos [1] and Panayiotis Vafeas [2]

[1] Department of Mechanical Engineering and Aeronautics, University of Patras, 26504 Patras, Greece; p.papadopoulos@des.upatras.gr
[2] Department of Chemical Engineering, University of Patras, 26504 Patras, Greece; vafeas@chemeng.upatras.gr
* Correspondence: panteleimonbakalis@upatras.gr

Abstract: We studied the laminar fully developed ferrofluid flow and heat transfer phenomena of an otherwise magnetic fluid into a vertical annular duct of circular cross-section and uniform temperatures on walls which were subjected to a transverse external magnetic field. A computational algorithm was used, which coupled the continuity, momentum, energy, magnetization and Maxwell's equations, accompanied by the appropriate conditions, using the continuity–vorticity–pressure (C.V.P.) method and a non-uniform grid. The results were obtained for different values of field strength and particles' volumetric concentration, wherein the effects of the magnetic field on the ferrofluid flow and the temperature are revealed. It is shown that the axial velocity distribution is highly affected by the field strength and the volumetric concentration, the axial pressure gradient depends almost linearly on the field strength, while the heat transfer significantly increases due to the generated secondary flow.

Keywords: ferrofluids; heat transfer; annular duct; magnetization equation; continuity–vorticity–pressure (C.V.P.); numerical method

Citation: Bakalis, P.A.; Papadopoulos, P.K.; Vafeas, P. Heat Transfer Study of the Ferrofluid Flow in a Vertical Annular Cylindrical Duct under the Influence of a Transverse Magnetic Field. *Fluids* **2021**, *6*, 120. https://doi.org/10.3390/fluids6030120

Academic Editors: Ioannis Sarris and Vyacheslav Akkerman

Received: 14 February 2021
Accepted: 11 March 2021
Published: 15 March 2021

1. Introduction

The examination of the characteristics of ferrofluids has generated much interest in past decades due to the many important technological applications [1–4]. The dispersion of a magnetizable mineral, such as an iron oxide powder, in a liquid solution, creates a fluid with unique properties such as magnetoviscosity [5–7] or negative viscosity [8], in the presence of a magnetic field. These properties can be exploited to create specialized engineering systems targeted for applications such as magnetic dampers [8] and shaft seals [9].

The numerical works that deal with ferrofluids usually focus on simple geometries, such as parallel plates and circular tubes, to facilitate the understanding of the complex phenomena that arise in these flows. The different timescales of the various physical mechanisms, i.e., the Brownian diffuse timescale, the hydrodynamic (convective) timescale and the timescale associated with applied magnetic field, are responsible for the non-equilibrium magnetization dynamics of the flow problem [10]. This variation in the relaxation time creates a misalignment between the local magnetization and the local magnetic field, leading to enhanced effective viscosity [11]. The interaction between the magnetic forces and the pressure gradient, apart from affecting the flow properties, induces changes in the flow pattern which may be utilized to control flow separation [12].

The numerical studies of ferrofluid flow focus also on geometries which are close to the actual engineering applications. The properties that are examined in this context are the pressure drop and heat transfer [13–15], while special attention is given to the velocity distributions that arise due to the interaction of the pressure gradients and the magnetic forces [16]. The flow and heat transfer characteristics of magnetic nanofluids have been compiled in a review paper [17] that discusses the properties of magnetic nano-fluids and their effect on natural convection, forced convection, and boiling. Specifically for thermal applications, annular pipes and double pipes are common configurations in heat exchangers, and their study is always interesting either in the case of ferrofluid flow or in neighboring scientific fields such as magnetohydrodynamics [18–20]. The utilization of different pipe shapes (e.g., sinusoidal or wavy [21]) and the inclusion of porous zones [22] in the flow passage can have a positive effect in heat transfer, although there is a penalty in pressure drop. Square ducts have also been reported in the bibliography [23], where flow takes place under the influence of transverse or axial magnetic fields. The different types of magnetic fields also play an important role in the flow properties and some of the configurations that have been examined are different types of magnets, such as quadrupole magnets [24], or current-carrying wires and coils [14,25]. An experimental study [26] showed that the use of ferrofluid flow in a circular pipe under the effect of a constant magnetic field can increase the heat transfer by up to 7.19%. Alternating magnetic fields are also important because they can enhance the heat transfer properties by up to 13.9% [13], when the frequency is optimum. Finally, the type of ferrofluid is an important element in the different configurations, with the most common being Fe_3O_4–water ferrofluids [27,28]. However, the range of applications is not restricted to engineering; there have been reports on the use of blood as ferrofluid [29,30].

In this context, the present work examines the ferrofluid flow of a magnetite–water solution in a vertical annular pipe. The magnetic field is constant and acts along the horizontal direction. This type of flow is important for cooling units and heat exchangers, and it can be employed in various engineering applications. The numerical model uses the formulation derived by Hatzikonstantinou and Vafeas [7] and the solution procedure is based on a validated in-house code. The main parameters that are studied are the magnetic field strength and the concentration of magnetic particles, which play an important role in the pressure drop, the velocity profiles and the heat transfer characteristics of the flow. To the best of our knowledge, this is the first work that examines the effects of these parameters in a forced convection problem with the inclusion of buoyancy effects. The results highlight the interaction between the gravitational, viscous, and magnetic forces, and provide useful information concerning the heat transfer augmentation that can be achieved.

2. Mathematical Model

We formulate our problem concerning the straight circular cylindrical annular duct, depicted in Figure 1, given the inner R_i and the outer R_o radii of the coaxial cylinders, wherein a conveniently adjusted Cartesian reference system (x, y, z) is sketched. The inner and outer cylinders are maintained at uniform temperatures, assuming that the inner wall temperature T_i is lower than the outer wall temperature T.

As for the developed buoyancy forces, the Boussinesq approximation is used, while the effect of viscous dissipation is neglected. On the other hand, the non-conductive ferrofluid is constituted by a stable suspension of solid spherical particles of radius r_p and density ρ_p with volumetric concentration $\phi = (4/3)\pi r_p^3 n$, where n stands for the number of particles per unit volume. They control the variation of the viscosity and the pressure of the ferrofluid, provided that an external magnetic field $\mathbf{H}_a$ is applied, as demonstrated in Figure 1. The best fitted circular cylindrical coordinate system (r, θ, z) with $r \in (R_i, R_o)$, $\theta \in [0, 2\pi)$ and $z \in (-\infty, +\infty)$ is implied, which is connected to the Cartesian coordinates via $(x, y, z) = (r\cos\theta,\ r\sin\theta,\ z)$.

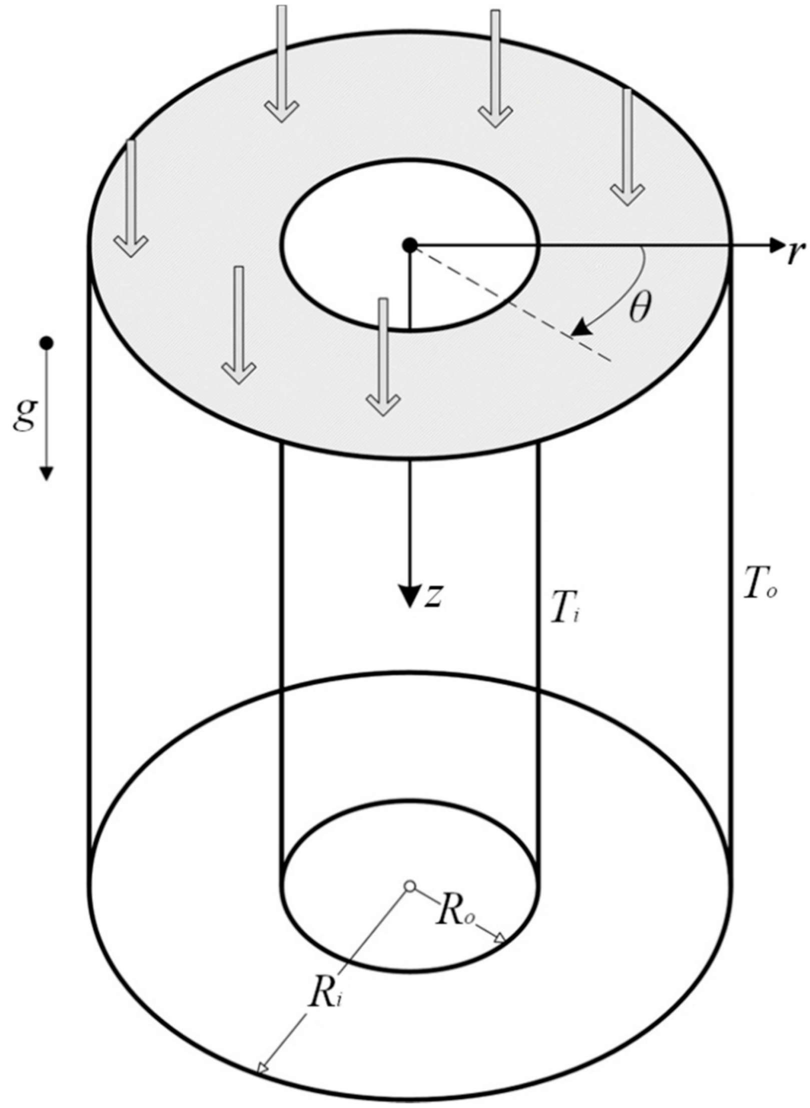

Figure 1. The coaxial system of the straight circular cylindrical annular duct.

In terms of the gradient ∇ and Laplacian Δ differential operators, the governing equations that describe the physical phenomenon of the particular ferrohydrodynamic flow within the annular duct with heat alterations, interconnect the velocity $\mathbf{v}$, the angular velocity $\mathbf{\Omega} = \nabla \times \mathbf{v}$, the total pressure P that incorporates the gravitational force, the magnetization $\mathbf{M}$, the magnetic field $\mathbf{H}$, which is the summation of the applied and the induced field, the latter being neglected, the magnetic induction $\mathbf{B}$ and the temperature $\mathbf{T}$. Each implicated physical field is then a function of the current position vector $\mathbf{r} = x\hat{\mathbf{x}} + y\hat{\mathbf{y}} + z\hat{\mathbf{z}}$, written in view of the Cartesian basis $\hat{\mathbf{x}}$, $\hat{\mathbf{y}}$, $\hat{\mathbf{z}}$ and the time variable t, omitting this dependence thereafter for notational clarity. Therein, supposing an incompressible Newtonian magnetic fluid with constant mass density ρ and with constant dynamic viscosity η, we introduce the following set of dimensional equations, which are comprised by the continuity equation:

$$\nabla \cdot \mathbf{v} = 0, \tag{1}$$

the momentum equation:

$$\rho \frac{D\mathbf{v}}{Dt} \equiv \rho \left[\frac{\partial \mathbf{v}}{\partial t} + (\mathbf{v} \cdot \nabla)\mathbf{v} \right] = -\nabla P + \eta \Delta \mathbf{v} + \mu_0 (\mathbf{M} \cdot \nabla)\mathbf{H} + \frac{\mu_0}{2} \nabla \times (\mathbf{M} \times \mathbf{H}) - \rho g \beta (T - T_i)\hat{\mathbf{z}}, \tag{2}$$

where μ_0 is the magnetic permeability of vacuum, g is the gravitational acceleration and β is the coefficient of thermal expansion, the energy equation:

$$\frac{D\mathbf{T}}{Dt} \equiv \left[\frac{\partial \mathbf{T}}{\partial t} + (\mathbf{v}\cdot\nabla)\mathbf{T}\right] = \frac{k}{\rho c_p}\Delta\mathbf{T}, \quad (3)$$

where k is the thermal conductivity and c_p is the specific heat, and the Maxwell's equations:

$$\nabla\cdot\mathbf{B} = 0 \text{ and } \nabla\times\mathbf{H} = 0, \quad (4)$$

where for a linear, homogeneous and isotropic fluid, it holds that $\mathbf{B} = \mu_0(\mathbf{H}+\mathbf{M})$. Those are supplemented by the magnetization equation:

$$\frac{D\mathbf{M}}{Dt} \equiv \frac{\partial\mathbf{M}}{\partial t} + (\mathbf{v}\cdot\nabla)\mathbf{M} = \frac{1}{2}\mathbf{\Omega}\times\mathbf{M} + \frac{\mu_0\tau_S}{I}(\mathbf{M}\times\mathbf{H})\times\mathbf{M} - \frac{1}{\tau_B}\left(\mathbf{M} - M_0\frac{\mathbf{H}}{H}\right) \quad (5)$$

where M_0 denotes the equilibrium magnetization field, rendered by the Langevin function:

$$M_0 = nmL(\xi) \text{ with } L(\xi) = \coth\xi - \frac{1}{\xi}, \text{ where } \xi = \frac{\mu_0 mH}{KT}, \quad (6)$$

wherein m is the magnetic moment of a single particle, whose magnetization M_p is related to the saturation magnetization M_s via the relationship $M_s = \phi M_p = nm$. Otherwise, $\tau_S = r_p^2\rho_p/15\eta_0$ is the relaxation time of particle rotation (η_0 corresponding to the rotational viscosity), $I = 8\pi r_p^5\rho_p n/15$ is the sum of moments of inertia of the spherical particles per unit volume and $\tau_B = 4\pi\eta r_p^3/KT$ is the relaxation time of the Brownian rotation (K being the Boltzmann's constant). However, due to the approximate homogeneity of the magnetic field and the very small magnetization inertia of the magnetic fluid, resulting in the almost immediate orientation of the magnetization leads to $D\mathbf{M}/Dt \cong 0$, so that partial differential Equation (5) becomes algebraic and is simplified to the analytical formula:

$$\mathbf{M} = \frac{M_0}{H}\left[1+\left(\frac{\Omega\,\tau_B}{2f(H,\Omega)}\right)^2\right]^{-1}\left\{\mathbf{H} + \frac{\tau_B}{2f(H,\Omega)}\mathbf{\Omega}\times\mathbf{H} + \left(\frac{\tau_B}{2f(H,\Omega)}\right)^2(\mathbf{H}\cdot\mathbf{\Omega})\mathbf{\Omega}\right\} \quad (7)$$

where $H = |\mathbf{H}|$ and $\Omega = |\mathbf{\Omega}|$. Using the dimensionless function:

$$g(H) = 1 + \frac{\mu_0\tau_S\tau_B}{I}HM_0, \quad (8)$$

it is readily obtained:

$$f(H,\Omega) = \frac{g(H)}{3}\left\{1 + R(H,\Omega) + \frac{1}{R(H,\Omega)}\left[1 - 3\left(\frac{\Omega\,\tau_B}{2g(H)}\right)^2\right]\right\} \quad (9)$$

with:

$$R(H,\Omega) = \left\{Q_\varphi(H,\Omega) + \sqrt{Q_\varphi^2(H,\Omega) - \left[1-3\left(\frac{\Omega\,\tau_B}{2g(H)}\right)^2\right]^3}\right\}^{1/3}, \quad (10)$$

in which, bearing in mind that φ is the angle between the magnetic field $\mathbf{H}$ and the vorticity $\mathbf{\Omega}$, which is $\mathbf{\Omega}\cdot\mathbf{H} = \Omega H\cos\varphi$, then:

$$Q_\varphi(H,\Omega) = 1 + \left(\frac{3\Omega\,\tau_B}{2g(H)}\right)^2\left[1 - \frac{3(g(H)-1)}{2g(H)}\sin^2\varphi\right], \quad (11)$$

providing adequate information to compute Equation (7). In summary, we are obliged to solve the continuity Equation (1), the momentum law (Equation (2)), the energy

Equation (3), Maxwell's relationships (Equation (4)) and, instead of Equation (5), the analytical form for the magnetization of the ferrofluid given by Equation (7), taking into account Equations (6) and (8)–(11). Those are accompanied by the non-slip boundary conditions for the velocity field, i.e., $\mathbf{v} = 0$ and the imposition of the standard temperatures T_i and T on both the walls of the annular duct for $r = R_i, R_o$, as well as implying the excitation through the magnetic field $\mathbf{H}_a$. Additionally, the flow is considered fully developed in the z-direction, while the magnetization on the boundaries can be recovered directly from the compact Equation (7).

The numerical implementation of the aforementioned boundary value problem requires the production of the corresponding dimensionless forms for all the involved equations. Following that, we define the dimensionless variables:

$$\begin{gathered}\widetilde{\mathbf{r}} = \frac{\mathbf{r}}{R_o}, \quad \widetilde{t} = \frac{Ut}{R_o}, \quad \widetilde{R} = \frac{R_i}{R_o}, \quad \widetilde{\nabla} = R_o\nabla, \quad \widetilde{\Delta} = R_o^2\Delta \\ \widetilde{\mathbf{v}} = \frac{\mathbf{v}}{U}, \quad \widetilde{P} = \frac{P}{\rho U^2}, \quad \widetilde{T} = \frac{T-T_i}{T_o-T_i}, \quad \widetilde{\mathbf{\Omega}} = \frac{R_o\mathbf{\Omega}}{U} \\ \widetilde{\mathbf{H}} = \frac{\mathbf{H}}{H_a}, \quad \widetilde{\mathbf{M}} = \frac{\mathbf{M}}{M_{s,\max}}, \quad \widetilde{M}_0 = \frac{M_0}{M_{s,\max}} = \phi L(\xi),\end{gathered} \tag{12}$$

where U is the mean velocity of the ferrofluid, $H_a = |\mathbf{H}_a|$ and $M_{s,\max}$ are the saturation magnetization for $\phi = 1$ and $H = H_a$, i.e., $M_{s,\max} = 3m/4\pi r_p^3$, because $M_s = nm$, given that $\phi = (4/3)\pi r_p^3 n$. By virtue of Equation (12), direct substitution to Equations (1)–(5) (or Equation (7) as the analytical counterpart of Equation (5) with Equations (8)–(11)) provides us with the dimensionless relationships of the continuity equation:

$$\widetilde{\nabla} \cdot \widetilde{\mathbf{v}} = 0, \tag{13}$$

the momentum equation:

$$\frac{\partial\widetilde{\mathbf{v}}}{\partial\widetilde{t}} + \left(\widetilde{\mathbf{v}} \cdot \widetilde{\nabla}\right)\widetilde{\mathbf{v}} = -\widetilde{\nabla}\widetilde{P} + \frac{1}{\mathrm{Re}}\widetilde{\Delta}\widetilde{\mathbf{v}} + \frac{\mathrm{R_M}}{\mathrm{Re}^2}\left[\left(\widetilde{\mathbf{M}} \cdot \widetilde{\nabla}\right)\widetilde{\mathbf{H}} + \frac{1}{2}\widetilde{\nabla} \times \left(\widetilde{\mathbf{M}} \times \widetilde{\mathbf{H}}\right)\right] - \frac{\mathrm{Gr}}{\mathrm{Re}^2}\ \mathrm{T}\ \hat{z}, \tag{14}$$

the energy equation:

$$\frac{\partial\widetilde{\mathbf{T}}}{\partial\widetilde{t}} + \left(\widetilde{\mathbf{v}} \cdot \widetilde{\nabla}\right)\widetilde{\mathbf{T}} = \frac{1}{\mathrm{RePr}}\Delta\widetilde{\mathbf{T}}, \tag{15}$$

the Maxwell's equations:

$$\widetilde{\nabla} \cdot \widetilde{\mathbf{B}} = 0 \text{ and } \widetilde{\nabla} \times \widetilde{\mathbf{H}} = 0 \tag{16}$$

and, additionally, either the differential form of the magnetization equation:

$$\frac{\partial\widetilde{\mathbf{M}}}{\partial\widetilde{t}} + \left(\widetilde{\mathbf{v}} \cdot \widetilde{\nabla}\right)\widetilde{\mathbf{M}} = \frac{1}{2}\left(\widetilde{\mathbf{\Omega}} \times \widetilde{\mathbf{M}}\right) + \frac{\mathrm{R_M}}{6\phi\mathrm{Re}}\left(\widetilde{\mathbf{M}} \times \widetilde{\mathbf{H}}\right) \times \widetilde{\mathbf{M}} - \frac{\mathrm{R_H}}{\mathrm{Re}}\left(\widetilde{\mathbf{M}} - \phi\frac{\widetilde{\mathbf{H}}}{\widetilde{H}}L(\xi)\right) \tag{17}$$

or its analytical expression:

$$\widetilde{\mathbf{M}} = \phi L(\xi)\frac{1}{\widetilde{H}\left(1 + \left(N\widetilde{\Omega}\right)^2\right)}\left[\widetilde{\mathbf{H}} + N\left(\widetilde{\mathbf{\Omega}} \times \widetilde{\mathbf{H}}\right) + N^2\left(\widetilde{\mathbf{\Omega}} \cdot \widetilde{\mathbf{H}}\right)\widetilde{\mathbf{\Omega}}\right] \tag{18}$$

Above are written in terms of the Reynolds, Grashof and Prandtl numbers:

$$\mathrm{Re} = \frac{\rho U R_o}{\eta},\ \mathrm{Gr} = \frac{g\beta(T_o - T_i)\rho^2 R_o^3}{\eta^2} \text{ and } \mathrm{Pr} = \frac{c_p\eta}{k}, \tag{19}$$

respectively, the dimensionless characteristic numbers:

$$\mathrm{R_M} = \frac{\mu_0\rho R_o^2 M_{s,\max} H_a}{\eta^2} \text{ and } \mathrm{R_H} = \frac{\rho R_o^2}{\eta\tau_B}, \tag{20}$$

as well as the known quantity:

$$N = \frac{\mathrm{Re}}{2\mathrm{R_H}}\left[\frac{q}{3}\left(1+R+\frac{1-3\left(\widetilde{\Omega}p\right)^2}{R}\right)\right]^{-1} \text{ with } p = \frac{\mathrm{Re}}{2\mathrm{R_H}g} \text{ and } q = 1+\frac{\mathrm{R_M}}{6\mathrm{R_H}}\widetilde{H}L(\xi), \quad (21)$$

where

$$R = \left[Q+\sqrt{Q^2-\left[1-3\left(\widetilde{\Omega}p\right)^2\right]^3}\right]^{\frac{1}{3}} \text{ with } Q = 1+9\left(\widetilde{\Omega}p\right)^2\left[1-\frac{3(q-1)}{2q}\left(\frac{\left|\widetilde{\mathbf{\Omega}}\times\widetilde{\mathbf{H}}\right|}{\widetilde{\Omega}\widetilde{H}}\right)^2\right], \quad (22)$$

concluding our dimensionless analysis. The cylindrical geometry is implied and $\widetilde{\mathbf{H}} \cong \mathbf{H}_a$ as for the physical assumption, although, because $\widetilde{r} = r/R_o$, the imposed boundary conditions read $\widetilde{\mathbf{v}} = 0$ for $\widetilde{r} = \widetilde{R}$ and $\widetilde{r} = 1$, as well as $\widetilde{T} = 0$ for $\widetilde{r} = \widetilde{R}$ and $\widetilde{T} = 1$ for $\widetilde{r} = 1$. On the other hand, because $\widetilde{z} = z/R_o$, the fully developed flow in the $\widetilde{z}$-direction is secured by the fact that are all the components of the fields are independent of the axial coordinate $\widetilde{z}$. Although the pressure field $\widetilde{P}$ is a linear function of z, all the axial derivatives are neglected, except for the axial pressure gradient $\widetilde{P}_{c,z} \equiv d\widetilde{P}_a(\widetilde{z})/d\widetilde{z}$, which is constant. Finally, $\widetilde{\mathbf{M}}$ on $\widetilde{r} = \widetilde{R}$ and $\widetilde{r} = 1$ is obtained via the analytical relationship in Equation (18), while the corresponding differential Equation (17) for the magnetization will be used for validation. In conclusion, a very important quantity is the stream function ψ ($\widetilde{\psi} = \psi/UR_o$ as for its dimensionless form), which is connected to the velocity components v_r and v_θ in cylindrical coordinates through the relationships:

$$v_r = \frac{1}{r}\frac{\partial\psi}{\partial\theta} \text{ and } v_\theta = -\frac{\partial\psi}{\partial r} \text{ or } \widetilde{v}_r = \frac{1}{\widetilde{r}}\frac{\partial\widetilde{\psi}}{\partial\theta} \text{ and } \widetilde{v}_\theta = -\frac{\partial\widetilde{\psi}}{\partial\widetilde{r}}, \quad (23)$$

wherein trivial integration techniques give the stream function in terms of the velocity field.

Heat transfer is studied with the Nusselt number. Local Nusselt numbers for the inner and outer wall are given by the relationships:

$$\mathrm{Nu_i} = \left.\frac{\partial\widetilde{T}}{\partial r}\right|_{\widetilde{r}=\widetilde{R}} \text{ and } \mathrm{Nu_o} = \left.\frac{\partial\widetilde{T}}{\partial r}\right|_{\widetilde{r}=1}, \quad (24)$$

while the average Nusselt numbers for the inner and outer wall are given by:

$$\overline{\mathrm{Nu_i}} = \frac{1}{2\pi}\int_0^{2\pi}\mathrm{Nu_i}(\theta)d\theta \text{ and } \overline{\mathrm{Nu_o}} = \frac{1}{2\pi}\int_0^{2\pi}\mathrm{Nu_o}(\theta)d\theta \quad (25)$$

Equations (14)–(18) that govern the ferrofluid and thermal flow were solved using a methodology involving the enhanced C.V.P. numerical variational method for the coupling of the continuity, the energy, the Navier–Stokes equation and the magnetization equation. In this method, the partial differential equations are discretized and solved numerically using a pseudo-transient marching algorithm. Non-uniform stretched meshes are used to accurately compute the thin boundary layers near the walls. The C.V.P. method's characteristics (extreme accuracy, robustness, easy convergence and easy implementation to complex geometries) make it unique for magnetic fluid applications. The numerical method is analytically presented and validated elsewhere [16]. The analytical solution of the magnetization equation for a ferrofluid flow inside a straight circular duct has also been validated previously [14].

3. Results and Discussion

Computations were carried out for a wide range of physical parameters of the ferrofluid flow for $\widetilde{R} = 0.5$. The relative flow, heat transfer and magnetization parameters varied in ranges, whereas $0 \leq \phi \leq 0.1$, $0 < \xi \leq 1$, $0 \leq \mathrm{Gr} \leq 10^3$, $\mathrm{Pr} = 6.8$, $\mathrm{Re} = 100$, $\mathrm{R_M} = 1.8 \times 10^{-4}$ and $\mathrm{R_H} = 2.77 \times 10^{-6}$. The numerical results are presented to illustrate the effect of the above parameters on the fluid flow and heat transfer to demonstrate the effect of the magnetic field on the velocity and temperature distribution.

The distributions of the axial velocity $\widetilde{v}_\zeta$ in the cross-sectional area of the annular duct are presented in the contour plots of Figure 2 for various values of ξ and Gr for concentration $\phi = 0.1$. For field strength $\xi = 0$, the distribution of the axial velocity is uniform, while as the Grashof number increases, the axial velocity peak is shifted to the inner wall, due to the effect of the buoyancy forces. For $\mathrm{Gr} = 0$, as the field strength ξ increases, the axial velocity is suppressed near the specific angles $\theta = 0°,\ 90°,\ 180°,\ 270°$ and its maximum value is redistributed in four symmetric poles near angles $\theta = 45°,\ 135°,\ 225°,\ 315°$. For $\mathrm{Gr} = 10^3$, due to the effect of the buoyancy forces, we have the formulation of another two poles at angles $\theta = 0°,\ 180°$, of which the values are decreased as the field strength increases.

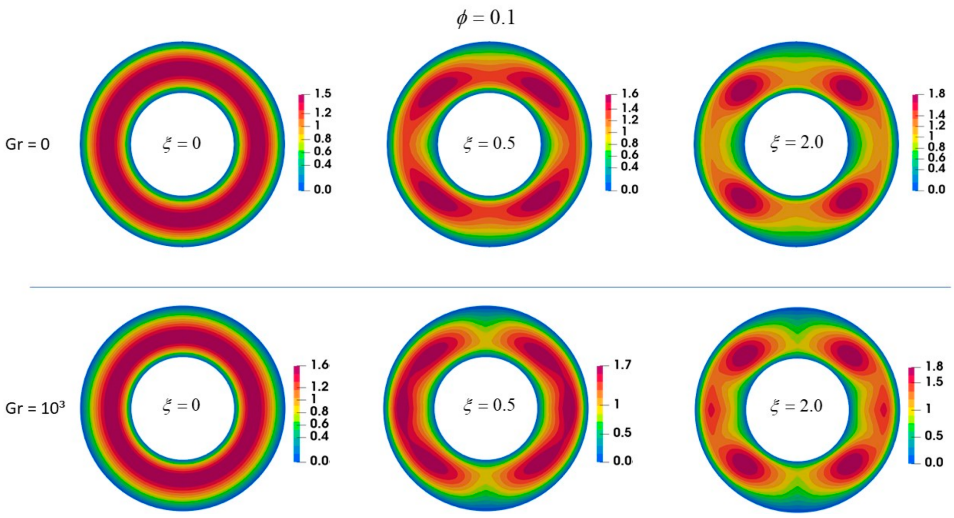

Figure 2. Contour plots of the axial velocity $\widetilde{v}_\zeta$ for various values of ξ and Gr for $\phi = 0.1$.

The contour plots of the streamlines of the transverse components of the velocity for various values of ξ and Gr and for concentration $\phi = 0.1$ are shown in Figure 3 Due to the effect of the field strength, the transverse components of the velocity form two pairs of vortices (one clockwise and one anticlockwise) on each region of the duct near angles $\theta = 45°,\ 135°,\ 225°,\ 315°$. As the field strength increases, the value of the stream function ψ also increases. Grashof number increase has a minor effect on the streamline values. Only for $\xi = 0.1$ is the absolute value of the stream function ψ slightly increased. For $\xi \geq 0.5$, the Grashof number has zero effect on the streamlines. This is due to the vertical alignment of the duct, because buoyancy forces are formulated in the axial direction.

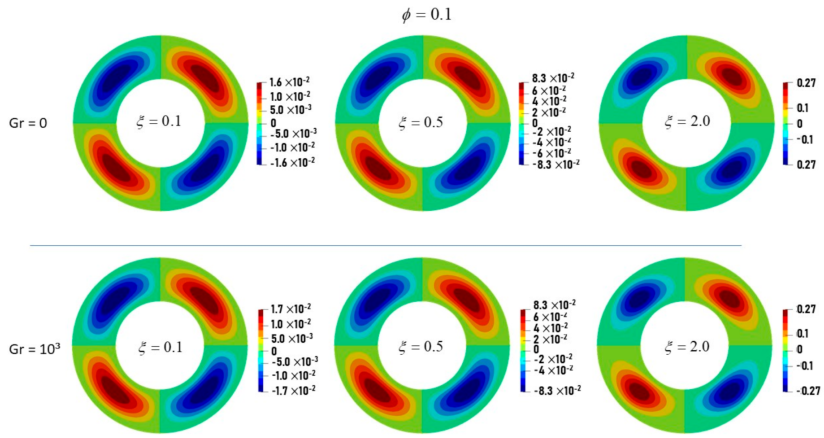

Figure 3. Contour plots of the streamlines ψ of transverse velocities $\widetilde{v}_r, \widetilde{v}_\theta$ for various values of ξ and Gr for $\phi = 0.1$.

The contour plots of the temperature for various values of ξ and Gr for concentration $\phi = 0.1$ are shown in Figure 4. For field strength $\xi = 0$, the distribution of the temperature is uniform. As the value of the stream function ψ increases due to the increase in the field strength, the temperature is redistributed. Temperature profiles are the same for both values of the Grashof number, because the secondary flow is not affected by the buoyancy forces.

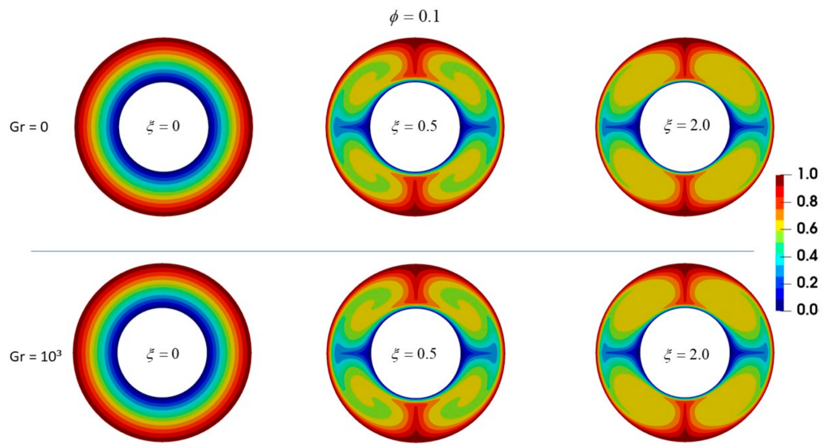

Figure 4. Contour plots of the temperature $\widetilde{T}$ for various values of ξ and Gr for $\phi = 0.1$.

Increasing the field strength ξ and concentration ϕ significantly improves the heat transfer at the walls, as expressed by the Nusselt number, due to the induction of the secondary flow. On the contrary, the increase in the Grashof number has a negligible effect on the heat transfer mechanism. As is presented in Figure 5, for $\phi = 0.01$, the heat transfer increases around 168% on the inner wall and 145% on the outer wall, for field strength $\xi = 2.0$ in comparison to $\xi = 0$. This effect is much higher for $\phi = 0.1$, where the heat transfer increases around 469% on the inner wall and 407% on the outer wall, for field strength $\xi = 2.0$ in comparison to $\xi = 0$.

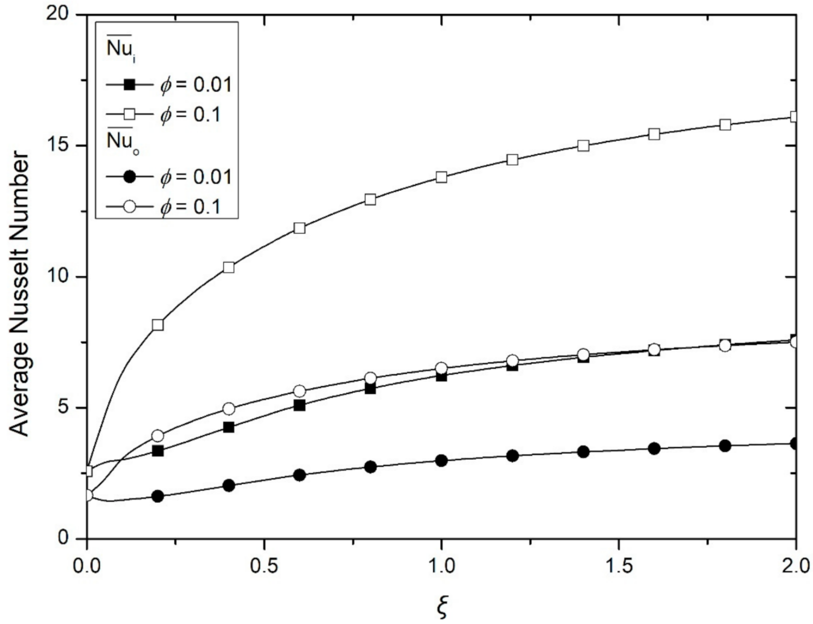

Figure 5. Effect of ϕ and ξ values on the average Nusselt number of the inner and outer cylinder for $Gr = 10^3$.

The required pump force for the ferrofluid flow is increased as the field strength and/or concentration increases, as is presented in Figure 6. For $\phi = 0.01$, the variation of the axial pressure gradient, as the field strength increases, is negligible, while for $\phi = 0.1$, field strength affects the axial pressure gradient. For $\xi = 2.0$, required pump force increases around 17% in comparison to $\xi = 0$. The effect of the Grashof number on the axial pressure gradient is much more significant. For $Gr = 10^3$, the axial pressure gradient is 107–120% higher in comparison to $Gr = 0$.

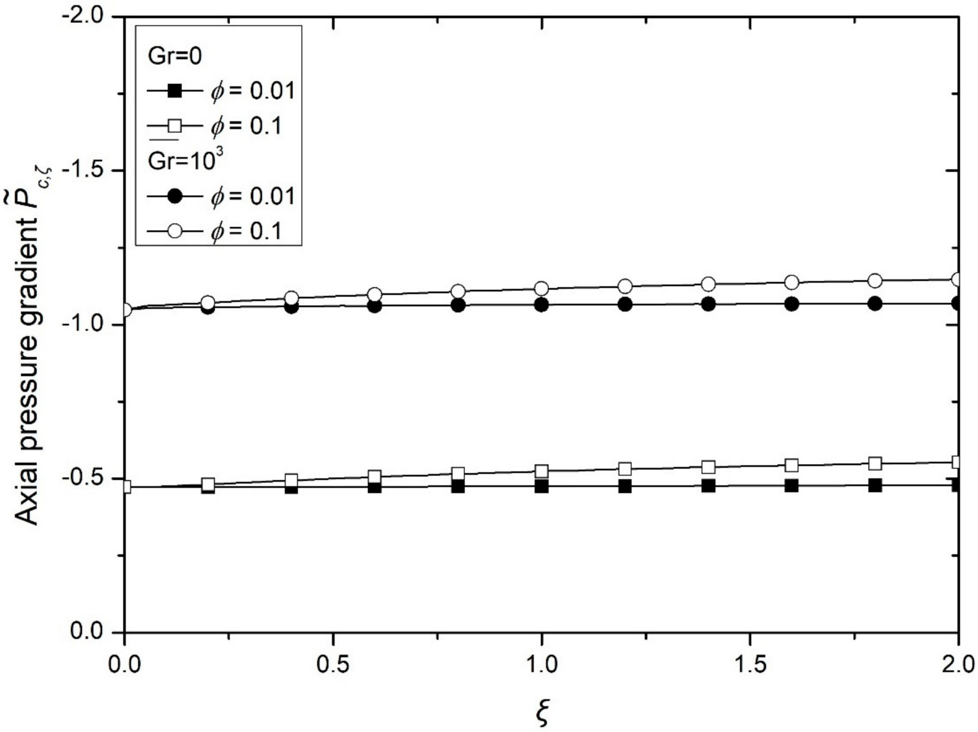

Figure 6. Effect of Gr, ϕ and ξ values on the axial pressure gradient $\widetilde{P}_{c,\zeta}$.

4. Conclusions

The effect of the magnetic field on the ferrofluid flow and the heat transfer in a vertical annular cylindrical duct has been studied in the present work. The numerical solution of the constitutive equations is based on the C.V.P. method, which is applied to a conveniently fixed cylindrical coordinate system. From the results, it is observed that the velocity distribution, heat transfer and pressure drop of the ferrofluid flow are highly affected by the external magnetic field and the concentration of magnetic particles. The axial flow is redistributed in four symmetric poles, where its maximum value is observed. A secondary flow is generated, due to the effect of the magnetic field, which significantly improves the heat transfer between the walls and the fluid. The axial pressure gradient, which is required to maintain the same mass flow, also increases as the field strength and concentration of magnetic particles increases, but with a lower rate in comparison to the increase in the heat transfer.

Author Contributions: Software, P.A.B.; methodology, P.K.P. and P.V.; visualization, P.A.B.; investigation, P.K.P.; writing—original draft preparation, P.A.B.; writing—review and editing, P.V. All authors have read and agreed to the published version of the manuscript.

Funding: This research received no external funding.

Institutional Review Board Statement: Not applicable.

Informed Consent Statement: Not applicable.

Conflicts of Interest: The authors declare no conflict of interest.

References

1. Berkovski, B.; Bashtovoy, V. *Magnetic Fluids and Applications Handbook*; Begell House: New York, NY, USA, 1996.
2. Gandomkar, A.; Saidi, M.H.; Shafii, M.B.; Vandadi, M.; Kalan, K. Visualization and comparative investigations of pulsating ferro-fluid heat pipe. *Appl. Therm. Eng.* **2017**, *116*, 56–65. [CrossRef]
3. Yamahata, C.; Chastellain, M.; Parashar, V.K.; Petri, A.; Hofmann, H.; Gijs, M.A.M. Plastic micropump with ferrofluidic actuation. *J. Microelectromech. Syst.* **2005**, *14*, 96–102. [CrossRef]
4. Bezaatpour, M.; Rostamzadeh, H. Heat transfer enhancement of a fin-and-tube compact heat exchanger by employing magnetite ferrofluid flow and an external magnetic field. *Appl. Therm. Eng.* **2020**, *164*, 114462. [CrossRef]
5. He, X.; Elborai, S.; Kim, D.; Lee, S.H.; Zahn, M. Effective magnetoviscosity of planar-Couette magnetic fluid flow. *J. Appl. Phys.* **2005**, *97*, 10Q302. [CrossRef]
6. Rosensweig, R.E. *Ferrohydrodynamics*; Dover Publications: New York, NY, USA, 1997.
7. Hatzikonstantinou, P.M.; Vafeas, P. A general theoretical model for the magnetohydrodynamic flow of micropolar magnetic fluids. Application to Stokes flow. *Math. Methods Appl. Sci.* **2010**, *33*, 233–248. [CrossRef]
8. Yang, W.; Wang, P.; Hao, R.; Ma, B. Experimental verification of radial magnetic levitation force on the cylindrical magnets in ferrofluid dampers. *J. Magn. Magn. Mater.* **2017**, *426*, 334–339. [CrossRef]
9. Kubik, M.; Pavliček, D.; MacHáček, O.; Strecker, Z.; Roupec, J. A Magnemorheological fluid shaft seal with low friction torque. *Smart Mater. Struct.* **2019**, *28*, 047002. [CrossRef]
10. Carvalho, D.D.D.; Gontijo, R.G. Magnetization diffusion in duct flow: The magnetic entrance length and the interplay between hydrodynamic and magnetic timescales. *Phys. Fluids* **2020**, *32*, 072007. [CrossRef]
11. Yang, W.; Liu, B. Effects of magnetization relaxation in ferrofluid film flows under a uniform magnetic field. *Phys. Fluids* **2020**, *32*, 062003. [CrossRef]
12. Ghosh, D.; Das, P.K. Control of flow and suppression of separation for Couette-Poiseuille hydrodynamics of ferrofluids using tunable magnetic fields. *Phys. Fluids* **2019**, *31*, 083609. [CrossRef]
13. Goharkhah, M.; Ashjaee, M. Effect of an alternating nonuniform magnetic field on ferrofluid flow and heat transfer in a channel. *J. Magn. Magn. Mater.* **2014**, *362*, 80–89. [CrossRef]
14. Papadopoulos, P.K.; Vafeas, P.; Hatzikonstantinou, P.M. Ferrofluid pipe flow under the influence of the magnetic field of a cylindrical coil. *Phys. Fluids* **2012**, *24*, 122002. [CrossRef]
15. Sheikholeslami, M.; Gerdroodbary, M.B.; Mousavi, S.V.; Ganji, D.D.; Moradi, R. Heat transfer enhancement of ferrofluid inside an 90° elbow channel by non-uniform magnetic field. *J. Magn. Magn. Mater.* **2018**, *460*, 302–311. [CrossRef]
16. Vafeas, P.; Bakalis, P.; Papadopoulos, P.K. Effect of the magnetic field on the ferrofluid flow in a curved cylindrical annular duct. *Phys. Fluids* **2019**, *31*, 117105. [CrossRef]
17. Bahiraei, M.; Hangi, M. Flow and Heat transfer characteristics of magnetic nanofluids: A review. *J. Magn. Magn. Mater.* **2015**, *374*, 125–138. [CrossRef]

18. Kakarantzas, S.C.; Sarris, I.E.; Vlachos, N.S. Natural Convection of liquid metal in a vertical annulus with lateral and volumetric heating in the presence of a horizontal magnetic field. *Int. J. Heat Mass Transf.* **2011**, *54*, 3347–3356. [CrossRef]
19. Kakarantzas, S.C.; Benos, L.T.; Sarris, I.E.; Knaepen, B.; Grecos, A.P.; Vlachos, N.S. MHD liquid metal flow and heat transfer between vertical coaxial cylinders under horizontal magnetic field. *Int. J. Heat Fluid Flow* **2017**, *65*, 342–351. [CrossRef]
20. Hatzikonstantinou, P.M.; Bakalis, P.A. A computational approach for the solution of the MHD and thermal flow of a liquid metal between two horizontal concentric cylinders. *Prog. Comput. Fluid Dyn. Int. J.* **2014**, *14*, 259–267. [CrossRef]
21. Mousavi, S.V.; Sheikholeslami, M.; Bandpy, M.G.; Gerdroodbary, M.B. The influence of magnetic field on heat transfer of magnetic nanofluid in a sinusoidal double pipe heat exchanger. *Chem. Eng. Res. Des.* **2016**, *113*, 112–124. [CrossRef]
22. Sheikhnejad, Y.; Ansari, A.B.; Ferreira, J.; Martins, N. Effects of parallel magnet bars and partially filled porous media on magneto-thermo-hydro-dynamic characteristics of pipe ferroconvection. *Int. J. Heat Mass Transf.* **2019**, *136*, 1273–1281. [CrossRef]
23. Aminfar, H.; Mohammadpourfard, M.; Zonouzi, S.A. Numerical study of the ferrofluid flow and heat transfer through a rectangular duct in the presence of a non-uniform transverse magnetic field. *J. Magn. Magn. Mater.* **2013**, *327*, 31–42. [CrossRef]
24. Bahiraei, M.; Hangi, M. Investigating the efficacy of magnetic nanofluid as a coolant in double-pipe heat exchanger in the presence of magnetic field. *Energy Convers. Manag.* **2013**, *76*, 1125–1133. [CrossRef]
25. Shakiba, A.; Vahedi, K. Numerical analysis of magnetic field effects on hydro-thermal behavior of a magnetic nanofluid in a double pipe heat exchanger. *J. Magn. Magn. Mater.* **2016**, *402*, 131–142. [CrossRef]
26. Sun, B.; Guo, Y.; Yang, D.; Li, H. The Effect of constant magnetic field on convective heat transfer of Fe_3O_4/Water magnetic nanofluid in horizontal circular tubes. *Appl. Therm. Eng.* **2020**, *171*, 114920. [CrossRef]
27. Hekmat, M.H.; Ziarati, K.K. Effects of nanoparticles volume fraction and magnetic field gradient on the mixed convection of a ferrofluid in the annulus between vertical concentric cylinders. *Appl. Therm. Eng.* **2019**, *152*, 844–857. [CrossRef]
28. Malekan, M.; Khosravi, A.; Zhao, X. The influence of magnetic field on heat transfer of magnetic nanofluid in a double pipe heat exchanger proposed in a small-scale CAES system. *Appl. Therm. Eng.* **2019**, *146*, 146–159. [CrossRef]
29. Tzirtzilakis, E.E.; Sakalis, V.D.; Kafoussias, N.G.; Hatzikonstantinou, P.M. Biomagnetic fluid flow in a 3D rectangular duct. *Int. J. Numer. Meth. Fluids* **2004**, *44*, 1279–1298. [CrossRef]
30. Ferdows, M.; Murtaza, M.G.; Tzirtzilakis, E.E.; Alzahrani, F. Numerical study of blood flow and heat transfer through stretching cylinder in the presence of a magnetic dipole. *ZAMM* **2020**, *100*, e201900278. [CrossRef]